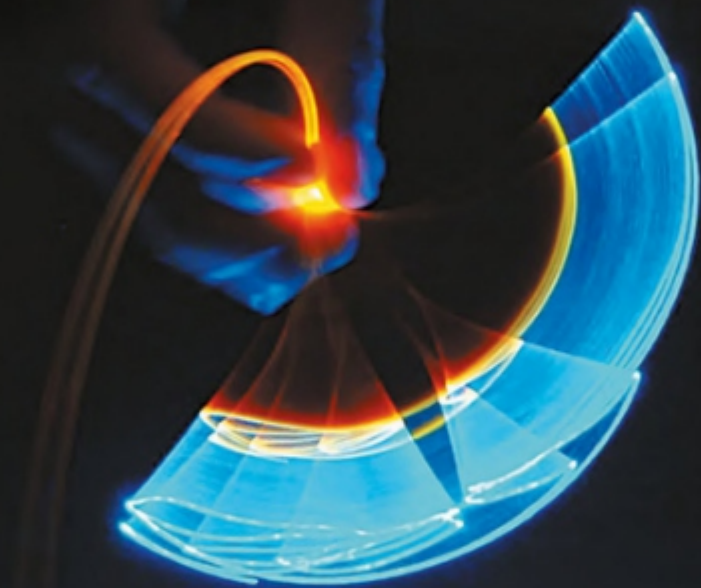# SHAPING
LIGHT IN NONLINEAR
OPTICAL FIBERS

EDITED BY
SONIA BOSCOLO • CHRISTOPHE FINOT

WILEY

14

Wide Variability of Generation Regimes in Mode-Locked Fiber Lasers

Sergey V. Smirnov,[1] Sergey M. Kobtsev,[1] and Sergei K. Turitsyn[2]

[1] *Novosibirsk State University, Novosibirsk, Russia*
[2] *Aston Institute of Photonic Technologies, School of Engineering and Applied Science, Aston University, Birmingham, UK*

14.1 Introduction

The evolution of modern laser systems necessarily involves an improvement in the output radiation parameters required by applications, with a parallel simplification of handling and operation. More and more laser products are adopting the black box approach, delivering an adjustment- and maintenance-free user experience with the ability to control the laser parameters electronically. Until very recently, these features were achievable only in lasers with a quite basic optical layout, but today, many hands-off maintenance-free lasers incorporate complex optical configurations, generate ultra-short radiation pulses, and boast very long lifetimes. These features, which were until only recently no more than wishful thinking, very largely became a reality due to fiber-optical technologies, the added benefits of which include relatively high efficiency and a small footprint. This progress is due to both advances in materials science and optical engineering and a better understanding of the complex physics underlying the operation of laser systems. Mode-locked fibre lasers (MLFL) have now become an indispensable tool in fundamental research and an integral part of many technological processes. They are widely used in an extensive application field, including material processing, spectroscopy, two-photon microscopy, ophthalmology, and may other promising applications.

Mode-locked lasers emerged at the very dawn of the laser epoch. The first report of mode locking a He-Ne laser with the help of an acousto-optical modulator was published more than half a century ago [1]. Passive mode locking of a continuous-wave laser via a saturable absorber was not achieved until almost 10 years later [2]. In a dye laser using Rhodamine 6G, spectrally limited 1.5-ps pulses were generated and spectrally tuned within the range of 590–610 nm. A diethyloxadicarbocyanine solution in methanol was employed as a saturable absorber in [2].

One decade later, research was under way in mode-locked fibre lasers. One of the first publications on the subject [3] reported 1-ns pulses with energy of 17 pJ generated in a

Nd-doped fibre laser. Within a few years, the ensuing attempts to shorten the duration of the generated pulses had led to orders-of-magnitude reduction, first to 90 ps [4], soon followed by a 4-ps result [5].

The past 50 years have witnessed profound progress in mode locking approaches. A large number of passive mode locking techniques were proposed and successfully implemented in lasers of different types: gas, solid-state, dye, diode, fiber lasers. Temporal compression of pulses generated in passively mode-locked solid-state lasers culminated in the achievement of attosecond pulse duration range ($1 \, \text{as} = 10^{-18}$ sec). For fiber lasers, typical pulse duration values lie in the range of several hundred femtoseconds, although the best achieved results reach 10–20 fs. Generation of ultra-short pulses in fiber lasers is anything but simple because of high nonlinearity and large chromatic dispersion of group velocities in fiber resonators. Nevertheless, these lasers feature a number of undeniable advantages in comparison with other laser types, being robust, compact, and efficient coherent light sources. All this draws a great deal of attention to ultra-fast fiber lasers in relation to multiple applications such as supercontinuum generation and optical metrology, spectroscopy, microscopy, processing and characterization of nano- and meta-materials. Fiber beam delivery provides the most convenient way of transporting laser radiation to the point of application, a critically important circumstance in ophthalmology and several other biomedical applications of ultra-short pulses. This stresses once more the importance of studying the science of complex laser systems, treating lasers not only as an engineering device, but also as a nonlinear physical system.

Apart from important practical applications, mode-locked fiber lasers exhibit quite a fascinating physics of formation and propagation of ultra-short pulses in optical fibers. This chapter explores the diversity of generation regimes observed in passively mode-locked fiber lasers, which may take place both in different lasers relying on different configurations for the generation of ultra-short pulses and in a single continuously operating laser device while the parameters of its cavity are adjusted.

Before proceeding to the main subject of the properties and diversity of generation regimes, let us briefly summarize the basic principles and approaches used for passive mode locking in order to generate ultra-short pulses in fiber laser cavities.

By creating optical feedback, a laser resonant cavity selects from electromagnetic radiation so-called modes: intrinsic, or natural, oscillations of the internal electromagnetic field. The frequencies of longitudinal modes are governed by the requirement that the cavity length be a multiple of an integer or half-integer number of wavelengths, and the frequency difference of adjacent longitudinal modes depends on the cavity length. For a linear 10–20-m-long cavity (the typical length of a fiber laser resonator), the frequency difference of neighboring longitudinal modes amounts to 15–7.5 MHz. Provided that all the optical elements of the fiber laser allow generation over the entire spectral gain range (it may be as wide as 100 nm), the number of laser modes present in the laser's generation spectrum may reach enormous values of $\sim 10^6$. If the phases of individual laser radiation modes are independent of each other or of an external common factor, the output of such a laser is continuous and, in relation to statistical properties, approaches that of band-pass-filtered incandescent and other thermal light sources. A great number of continuous fiber lasers operate in this regime.

In order to achieve pulsed generation, it is necessary to either directly create temporally localized light waves inside the resonator (Q-switching, gain switching, or synchronous pumping technologies) or establish a correlation between individual modes of

the laser cavity by applying active or passive mode locking. Methods of active mode locking are based on RF-driven acousto-optical modulation of either optical losses or phase incursion of intra-cavity radiation. This approach allows the generation of short (usually in the nano- and pico-second range of duration) laser pulses. In this chapter, however, we will mostly focus on passively mode-locked fiber lasers capable of producing even faster pico- and femto-second pulses. Passive mode locking relies on the introduction into the laser cavity of a saturable absorber, an optical element (or a group of elements), in which the optical losses depend on the intensity of the intra-cavity radiation in such a way that at higher intensities they become lower (saturate). This facilitates formation in the cavity of pulses with relatively high power and ensures the suppression of noise and continuous radiation components. Note that in terms of nonlinear science, the pulse is formed from linear dispersive waves due to the interplay between nonlinearity and dispersion (with the possible involvement of other effects) leading to light localization.

To date, passive mode locking in fiber lasers has been achieved through saturable absorbers based on a great number of different materials including carbon nano-tubes [6–12], graphene [13–15], molybdenum disulphide (MoS_2) [16,17], tungsten disulphide (WS_2) [18,19], topological isolators [20,21], and semiconductor saturable absorber mirrors (SESAM) [22–26].

In order to generate laser pulses with relatively high energy and peak power, it is advantageous to employ artificial saturable absorbers such as nonlinear optical loop mirrors (NOLM) [27]or nonlinear amplifying loop mirrors (NALM) [28] and nonlinear polarization evolution effect (NPE) [29]. In comparison to material-based saturable absorbers, these methods ensure a much longer lifetime and a much higher thermal damage threshold, thus allowing relatively high output pulse energies in passively mode-locked lasers without resorting to additional optical amplification [30–35]. Systems relying on artificial saturable absorbers also offer a unique possibility (discussed in more detail further on) of absorber parameter adjustment. The parameters of the output radiation are controlled through adjusting the power level of the optical pump, as well as the settings of the intra-cavity polarization controllers and/or phase plates. Though often more complex for understanding and handling, these methods potentially provide access to a very broad range of generated pulse parameters.

14.2   Variability of Generation Regimes

In our study of the variety of fiber laser generation regimes, we will rely on the numerical modeling of a ring fiber laser passively mode-locked due to the effect of nonlinear polarization evolution. This particular type of laser configuration was selected as a test bed because of its two polarization controllers defining the action of the artificial saturable absorber and offering a great number of degrees of freedom affecting the laser generation regime. The optical layout of the modeled laser is similar to those used in our previous studies [36–38], see Figure 14.1. The fiber laser has a ring cavity with a wave-division multiplexer (WDM) used to couple in the pump radiation. Either 2-m-long Er- or 8-m-long Yb-doped optical fiber is used in different experiments as the active medium, both of which produce qualitatively similar results at net-normal and all-normal cavity dispersion respectively. Either SMF-28 or normal-dispersion fiber (NDF) is used to elongate the cavity and thus increase pulse energy. Output laser radiation is
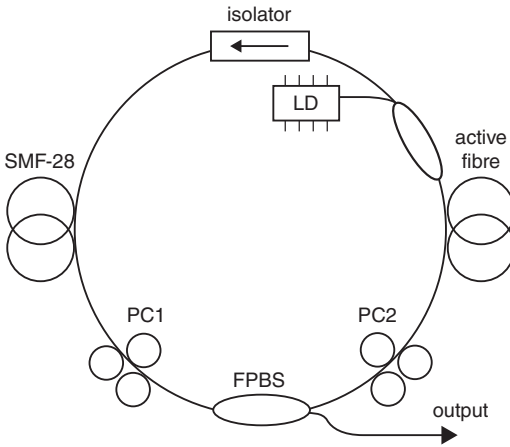
Figure 14.1 Laser layout used in experiments.
Key: LD laser diode, FPBS fibre polarization beam splitter; PC1, 2 fibre polarization controllers.

extracted through a fiber polarization beam splitter (FPBS) or through an additional coupler inserted into the cavity. Mode-locked operation was achieved by adjusting fiber polarization controllers PC1, 2. Operation regimes were studied with the help of a fast oscilloscope, an optical spectrum analyser (OSA), and an optical pulse auto-correlator.

In order to investigate the variety of possible single-pulse lasing regimes (the generation of only one pulse/train during laser cavity round trip) and their properties, we used a well-established numerical model based on a set of modified nonlinear Schrödinger equations for the orthogonal polarization components of the field envelope [39]:

$$\frac{\partial A_x}{\partial z} = i\gamma \left\{ |A_x|^2 A_x + \frac{2}{3}|A_y|^2 A_x + \frac{1}{3}A_y^2 A_x^* \right\} + \frac{g_0/2}{1 + E/(P_{sat} \cdot \tau)}A_x - \frac{i}{2}\beta_2 \cdot \frac{\partial^2 A_x}{\partial t^2} \quad (14.1)$$

$$\frac{\partial A_y}{\partial z} = i\gamma \left\{ |A_y|^2 A_y + \frac{2}{3}|A_x|^2 A_y + \frac{1}{3}A_x^2 A_y^* \right\} + \frac{g_0/2}{1 + E/(P_{sat} \cdot \tau)}A_y - \frac{i}{2}\beta_2 \cdot \frac{\partial^2 A_y}{\partial t^2} \quad (14.2)$$

where A_x, and A_y are the polarization components of the field envelope, z is the longitudinal coordinate along the fiber, t – time in the retarded frame of reference, γ and β_2 are nonlinear and dispersion coefficients correspondingly, g_0 and P_{sat} stand for unsaturated gain coefficient and saturation power for the active fiber.

Equations (14.1 and 14.2) describe the propagation of radiation along an active fiber. Taking $g_0 = 0$, we can use the same equations to model laser pulse propagation inside a passive resonator fiber. The fiber-optical polarization beam splitter is represented in the model by the following matrix:

$$\hat{T}_{PBS} = \begin{pmatrix} 1 & 0 \\ 0 & 0 \end{pmatrix}. \quad (14.3)$$

Unitary 2×2 matrices must be used to describe polarization controllers. In particular, a polarization controller based on the principle of fiber compression in the direction at an angle φ can be expressed as a matrix introducing phase delay α rotated by angle φ by multiplying it by the corresponding rotation matrix:

$$\hat{T}_{PC1}(\alpha, \varphi) = \begin{pmatrix} \cos\varphi & -\sin\varphi \\ \sin\varphi & \cos\varphi \end{pmatrix} \begin{pmatrix} e^{i\alpha/2} & 0 \\ 0 & e^{-i\alpha/2} \end{pmatrix} \begin{pmatrix} \cos\varphi & \sin\varphi \\ -\sin\varphi & \cos\varphi \end{pmatrix} \quad (14.4)$$

The parameter α in Eq. (14.4) stands for the phase delay introduced by the polarization controller and depends on the transverse fiber deformation. Similarly, a polarization controller using fiber torsion can be expressed through its eigenvector projections: $\hat{T}_{PC2} = e^{i\alpha/2}\hat{P}_+ + e^{-i\alpha/2}\hat{P}_-$, where the circular polarization state projections can be written as

$$\hat{P}_\pm = \frac{1}{2}\begin{pmatrix} 1 & \mp i \\ \pm i & 1 \end{pmatrix}. \tag{14.5}$$

In order to model the propagation of laser pulses around the fiber cavity, Eqs. (14.1 and 14.2) can be integrated numerically by the step-split Fourier method [39]. At the required points along the optical path, the polarization transformations (3–5) are applied and losses corresponding to the intra-cavity elements are taken into account.

This modeling cycle is carried out repeatedly until a stationary state is reached. As a rule, it takes between several hundred and several thousand modeled cavity round trips to reach the asymptotic state, depending on the system parameters and the initial conditions, taken here as white noise or seed pulses. In certain cases, a laser may exhibit bi-stability: the limit cycle of the propagation equations may depend on the initial conditions. It is relevant to mention here that a similar phenomenon is observed in experiment as hysteresis in switching between generation regimes [40]. When the limit cycle of the propagation equations corresponds to the "conventional" pulse generation regime, the generation parameters (power, pulse duration, spectrum width, etc.) of the limit cycle are highly stable (of the 10^{-3} order and better). Conversely, when the laser generates double-scale pulses (regular trains of pico- or nanosecond wave packets stochastically filled with femtosecond sub-pulses), the pulse parameters in the generated train fluctuate around their average values by a few percent or even more between two successive cavity round trips. This circumstance can be used in modeling as a basic criterion to tell apart generation regimes. We need to point out as well that the average generation parameters must be insensitive to variation within reasonable limits of the "non-physical" modeling parameters, such as the mesh node count, mesh width, and the step of numerical integration of Eqs. (14.1 and 14.2). This has to be controlled during modeling.

The laser layout depicted in Figure 14.1 includes two fiber polarization controllers, which provide several degrees of freedom, including the ability to trigger the mode-locked operation and then switch between different generation regimes or adjust laser parameters. Since investigation of laser properties in multi-dimensional space is quite complicated, we confine ourselves to a statistical study of different generation regimes. The approach consists of choosing the polarization controller settings (tilt/slew angles) in a random way and integrating Eqs. (14.1 and 14.2) with white noise as the initial conditions. After a certain number (typically $10^2 \ldots 10^4$) of round trips, we may obtain one of the following solutions: (i) quasi-CW laser operation (no mode-lock reached; thus Eqs. (14.1 and 14.2) and their numerical solution are not valid); (ii) multi-pulse mode-locked operation (that is, two or more pulses co-exist in the cavity); and (iii) single-pulse, mode-locked operation. If a single-pulse, mode-locked operation is reached after the fixed amount of cavity round trips, the program saves the results (tilt angles of PC1, 2, pulse duration, energy, optical spectrum, temporal intensity distribution, etc.). Otherwise, no information is kept about this program run. In either case, the program selects a new combination of random PC settings and proceeds with the next run, thus accumulating information about single-pulse operation regimes.

The lasing regimes found in simulation demonstrate both quantitative and qualitative differences. Qualitatively, one can distinguish two main types of single-pulse generation regimes: fully coherent "regular" pulses and partially coherent noise-like (double-scale) pulses with a complex inner structure [37]. The temporal distribution of the radiation intensity for fully coherent pulses features a smooth envelope and can be described by a single parameter, that is, the envelope width. In contrast, the temporal intensity distribution of the radiation of partially coherent pulses is stochastic: inside wave-packets with overall duration of several picoseconds to several nanoseconds; there are fast stochastic variations of radiation intensity with typical time scale of a hundred to several hundred femtoseconds.

Correspondingly, the temporal distribution of radiation intensity for noise-like pulses is defined by two temporal parameters: the pulse-train envelope width and the typical intensity fluctuation time inside the train. Overall parameters of the entire wave packet, such as bandwidth, energy, and duration, fluctuate around their average values within a wide range from one wave packet to another. Intensity fluctuations inside a single wave packet may also vary from relatively small values up to peak intensity of the pulse. Lasing regimes with strong intensity fluctuations are usually classified as noise-like generation.

Noise-like pulses have not yet received a universal designation. Different terms are found across the available literature: noise-like pulses [41, 42], double-scale lumps [37], femtosecond clusters [43], etc. These types of pulses can easily be identified by a singular auto-correlation function shape featuring a narrow (100–200 fs) peak on a broader picosecond pedestal. Significant attention to these pulses is predominantly due to the presence of femtosecond components with high peak power, while the cavities of fiber lasers generating them may have relatively large dispersion.

There is also a series of intermediate possibilities between "regular" laser pulses and noise-like generation which exhibits a relatively small and variable fraction of intensity noise and phase fluctuations on the background of single-scale laser pulses [36]. Remarkably, even inside a single type of lasing (i.e., "regular" or noise-like pulses), the studied laser supports a large variety of sub-regimes that correspond to different settings of PC1, 2 and thus differ vis-à-vis energy, duration, bandwidth, etc. Generated pulse parameters may vary by an order of magnitude or even more, depending on PC settings. Probability density functions (PDF) for rms-duration (see Figures 14.2 (a) and (b)) and rms- bandwidth (see Figure 14.2 (c), (d)) obtained by randomly changing simulation PC settings are shown in Figure 14.2. These PDFs reveal the extent of parameter variability in different realizations of two main single-pulse lasing regimes, namely "regular" lasing (Figures 14.2 (a) and (c)) and noise-like pulse generation (Figures 14.2 (b) and (d)). For instance, rms-bandwidth varied in random simulation runs from 0.2 up to 3.9 nm for "regular" pulses and from 0.3 up to 7.4 nm for noise-like pulses as a function of PC settings. (Note that the given values correspond to the pulse rms-bandwidth, which is usually several times as narrow as the spectrum's full width at half-maximum, FWHM. As an example, for a Π-shaped spectrum, the ratio between spectral FWHM and rms-bandwidth is 3.5. For differently shaped spectra, this ratio may vary.)

In addition, Figures 14.2 (e) and (f) show PDF for output pulse energy in 'regular' and noise-like pulse generation regimes respectively. Similarly to rms pulse duration, pulse energy may also vary by an order of magnitude when intra-cavity PC angles are changed, as can be seen in Figure 14.2.
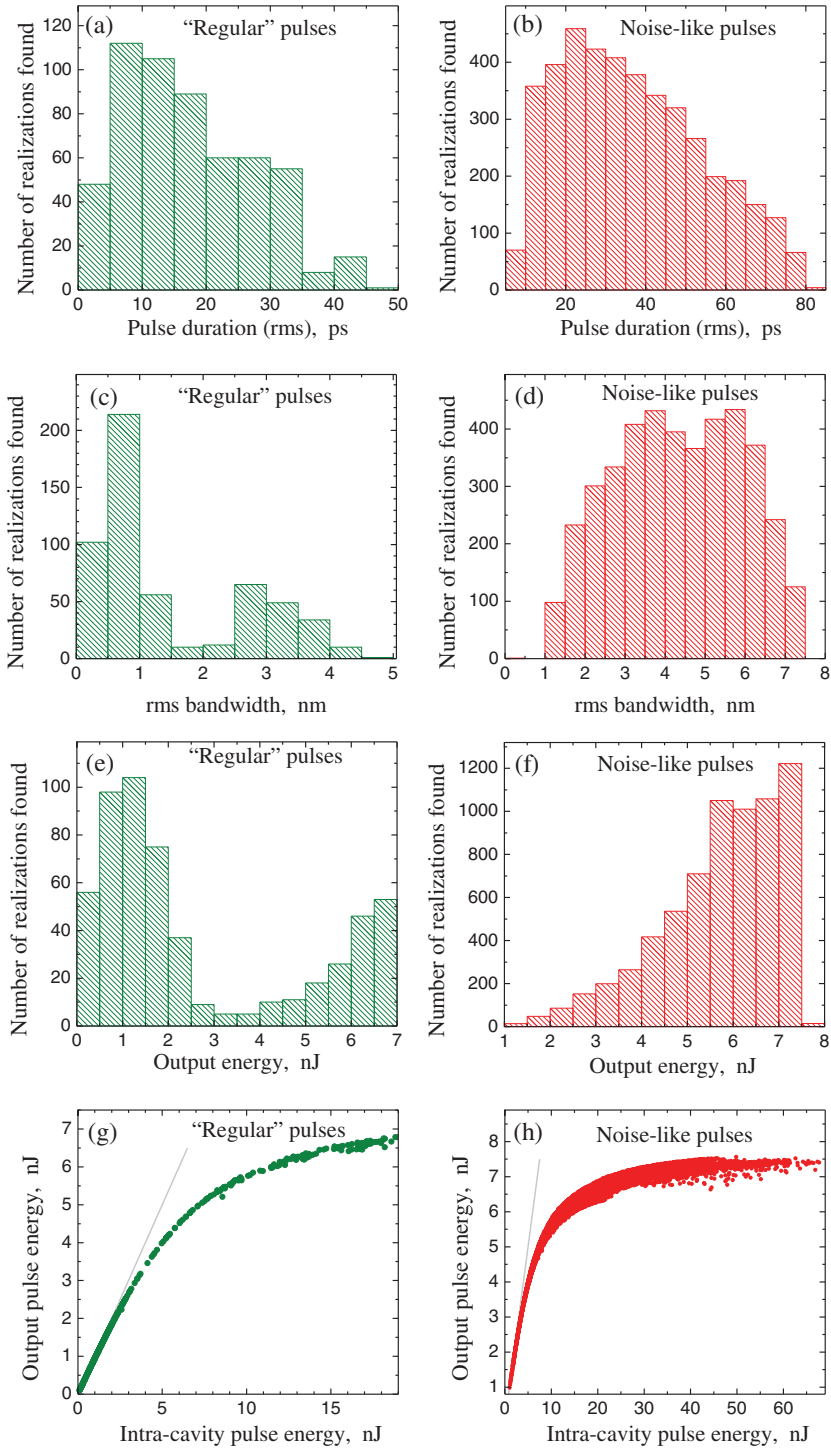
Figure 14.2 Variability in simulated "regular" and noise-like lasing regimes.

Highly different and widely ranging generation parameters in the studied fiber lasers passively mode-locked due to nonlinear polarization evolution (NPE) arise from the ability of the experimentalist to vary at will the properties of the artificial saturable absorber of an operating laser system by adjusting the intra-cavity polarization controllers. As an illustration, dots in Figures 14.2 (g) and (h) correspond to various "regular" (Figure 14.2 (g)) and noise-like (Figure 14.2 (h)) generation regimes identified in modeling and shown in coordinates intra-cavity pulse energy *vs.* output pulse energy. The gray solid line in these figures corresponds to $E_{out} = E_{in}$, which is achieved at 100% out-coupling of the intra-cavity radiation through the PBS. The observed spread of the angular coordinate of dots in these diagrams indicates that it is possible to control the amount of radiation coupled out of the cavity through PBS by adjustment of the intra-cavity polarization controllers.

Another important difference between lasing regimes attainable at different angular settings of intra-cavity PCs is related to the efficiency of nonlinear laser pulse conversion. Recently it was found that the efficiency of second harmonic generation (SHG) may vary by an order of magnitude or even more depending, along with other laser pulse parameters, on PC settings (see [38] and Figures 14.3 (a) and (b)). In order to generalize our conclusions, we study dimension-relative SHG efficiency ζ, which is defined [38] as

$$\zeta = \left(\sum_n \left| \sum_{j+k=n+1} A_{1j} A_{1k} \right|^2 \right) \cdot \left(\sum_j |A_{1j}|^2 \right)^{-2}.$$

In other words, ζ is the SHG relative efficiency which is equal to the ratio of two SH powers, of which the first is obtained when the nonlinear crystal is pumped by a double-scale laser pulse with given mode amplitudes A_{1j} and the second is generated with the use of single-mode monochromatic pumping of the same power $P_1 = \sum |A_{1j}|^2$. The dimensionless SHG relative efficiency ζ does not depend on the power and thickness of the thin nonlinear crystal but is sensitive to mode correlations and fluctuations, thus allowing us to easily compare different lasing regimes from the viewpoint of the efficiency of the nonlinear frequency.

As our simulation shows (see Figure 14.3 (c)), double-scale pulses have comparable or higher SHG-relative efficiency compared with that of single-scale laser pulses of the same duration. Figure 14.3 (d) shows the correlation between the SHG relative efficiency and spectral bandwidth of "regular" and noise-like laser pulses. It should be stressed that here we consider the case of a very thin crystal, so that the SHG efficiency tends to grow with the number of interacting spectral modes (and, as a result, with the spectral bandwidth of laser pulses).

We also conducted a comparative study of Raman scattering spectra generated by single-scale and double-scale laser pulses in a long stretch of extra-cavity fiber. As is illustrated below, notwithstanding the similar duration of single-scale and double-scale pulse envelopes, Raman spectra resulting from these pulses are substantially different.

Shown in Figures 14.4 and 14.5 are the radiation spectra and auto-correlation functions (ACF) of single-scale and double-scale pulses studied in our experiment. Pulses of both types were generated in the laser cavity of Figure 14.1 at different polarization
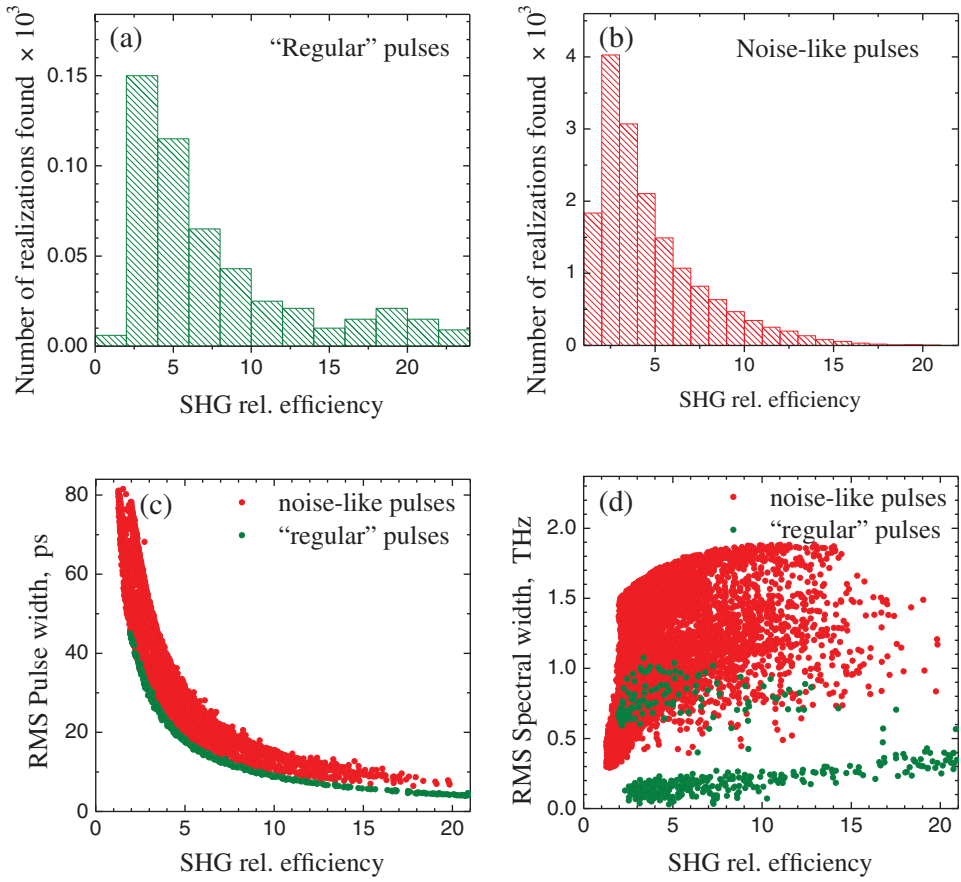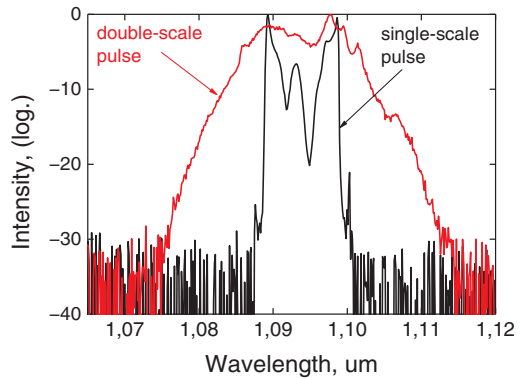
Figure 14.3 Relative SHG efficiency in "regular" (a) and noise-like (b) generation regimes and its correlation with rms pulse duration (c) and spectral width (d).

Figure 14.4 Radiation spectra of single-scale and double-scale pulses used in the experiment.
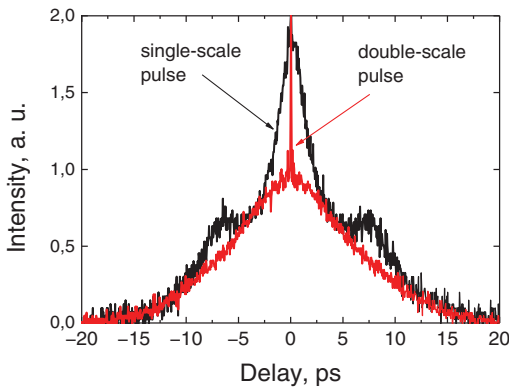
Figure 14.5 Auto-correlation functions of single-scale and double-scale pulses used in the experiment.

controller positions. ACFs were registered using commercial femto- and picosecond scanning auto-correlator "Tekhnoscan FS-PS-Auto." Auto-correlation traces appear to have a certain amount of noise, an effect caused by the optical power being insufficient for reliable detection. Optical spectra were measured with optical spectrum analyser Advantest Q8381A. Laser regimes were self-started and could be triggered by appropriate adjustment of PC and pump power (in the range of 1.3 and 1.5 W). Experimental results are in good qualitative agreement with the numerical simulation. Single-scale pulses have Π-shaped optical spectrum and quasi-bell-shaped ACF, whereas the spectrum of double-scale pulses is much smoother, bell-shaped, and its ACF contains a narrow (180-fs-wide) peak on a 12-ps-wide pedestal.

Figure 14.6 shows the Raman scattering spectra of single-scale (gray curves) and double-scale (black curves) pulses propagating along a 1.2-km long phosphosilicate fiber. In order to produce sufficient spectral conversion, pulses from the master fiber oscillator could be passed through a fiber optic amplifier to reach the average output power of 840 mW. This figure presents broader Raman scattering spectra of double-scale pulses in comparison to analogous spectra for single-scale pulses. Most likely, this is a result of femtosecond components present in the structure of double-scale pulses, which have higher nonlinear conversion efficiency.
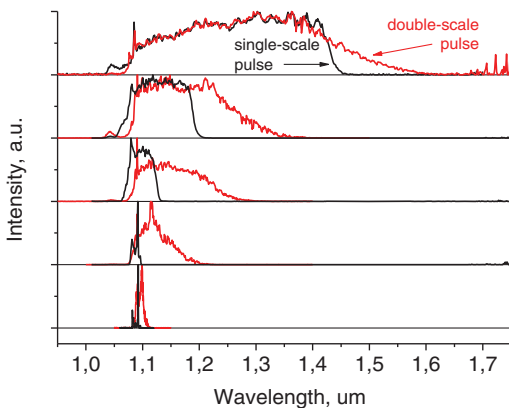

Figure 14.6 Raman radiation spectra from 1.2-km-long phosphosilicate fiber pumped with single-scale and double-scale pulses.

14.3   Phenomenological Model of Double-Scale Pulses

As was mentioned above, lasing regimes generating noise-like pulses may be used in a number of applications due to their particular properties, such as high peak power and low coherence time. The list of promising applications of noise-like pulses includes nonlinear frequency conversion, such as harmonic generation [38], Raman conversion [44, 45] and super-continuum generation [46–51], as well as applications in imaging and sensing systems with high temporal and/or spatial resolution. Excessive noise level intrinsic to noise-like pulses may constitute an obstacle for pulse compression [36, 52]. However, noise is known to play an important role in both supercontinuum generation [53–55] and Raman conversion, including soliton self-frequency shift effect [56–58] where noise may not only deteriorate SC coherence but also boost spectral broadening. It was furthermore demonstrated that the generation of noise-like pulses in long lasers represents a remarkably multiform phenomenon encompassing many nonlinear optical mechanisms, whose interaction may result in the emergence of diverse spatio-temporal coherent structures in laser radiation [59].

In order to benefit from noise-like pulses in various applications of laser physics, extensive numerical simulations are required. Here we propose a fairly simple phenomenological model of noise-like pulses, which is much easier to implement than the full-vector NLSE-based model used earlier. Since this model has a number of free parameters, it allows one to describe a large variety of lasing regimes achievable in experiments. Furthermore, this model helps one to obtain deeper insight into the nature of noise-like pulses by revealing their stochastic and deterministic properties.

The proposed simplified model of "random pulses" is constructed in two steps as follows. (i) Let us consider stochastic continuous radiation resulting from the superposition of a large number of uncorrelated modes within a given bandwidth. (ii) Let us shape the pulse by multiplying this stochastic quasi-CW radiation by a pulse envelope, for example, Gaussian pulse $\exp(-(t/T)^2 \ln 4)$, where T is the pulse full-width at half maximum (FWHM) and ln denotes natural logarithm. As a result, the random pulse envelope can be represented as

$$A(t) \sim \sqrt{P(t)} \cdot \sum_j A_j \exp(i\omega_j t). \tag{14.6}$$

Here, ω_j is the frequency of the j-th mode, t = time, A_j = complex amplitude of the j-th mode, $P(t)$ = temporal profile of the 'random' pulse, and $P(t) = \exp(-(t/T)^2 \, 4 \ln 2)$. The phases of complex amplitudes $\arg\{A_j\}$ are taken as independent random variates uniformly distributed from 0 to 2π. Physically "random pulses" Eq. (14.6) may appear, for example, as a result of temporal shaping of spectrally filtered radiation of a light bulb. Let us compare the properties of such "random pulses" with those of noise-like pulses obtained in an NLSE-based model of a fiber laser.

First of all, let us consider the temporal intensity distributions shown in Figures 14.7 (a) and (b) for some random realization of Eq. (14.6) and for some random realization of noise-like pulses obtained in NLSE-based modeling respectively. Both temporal intensity distributions shown in Figure 14.7 (a) and Figure 14.7 (b) consist of numerous sub-pulses filling a bell-shaped envelope of a wave-packet. Note that in this particular case, the wave-packet envelope is Gaussian, however, any particular pulse shape $P(t)$ known
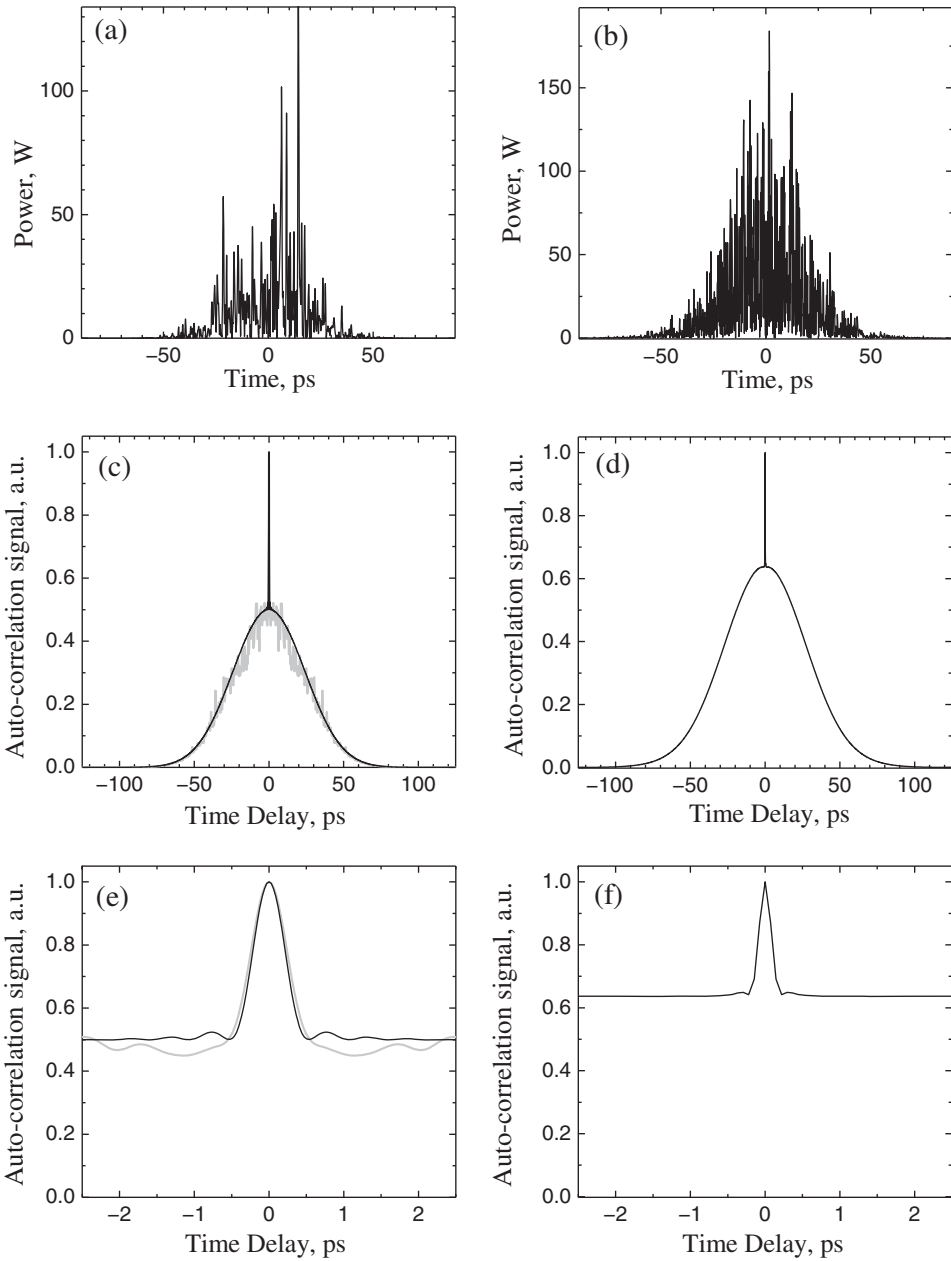
Figure 14.7 Temporal intensity distributions (a, d) and intensity auto-correlation functions (b, c, e, f) of "random" pulses (upper row, a, b, c) and noise-like pulses (lower row, d, e, f). Panels (c) and (f) illustrate the central ACF peak magnified from graphs (b) and (e) respectively.

from experiment may be used within the considered model in Eq. (14.6). Sub-pulses inside a wave-packet are located chaotically having random durations and amplitudes. Note that the duration of these sub-pulses is in the femtosecond range so that they cannot be directly resolved by oscilloscope in experiment. In most experimental configurations, the presence of such sub-pulses inside a wave-packet manifests itself as a narrow (femtosecond) peak on ACF. Figures 14.7 (c, d) show ACFs of a "random" pulse Eq. (14.6) and a noise-like pulse obtained in NLSE-based modeling respectively. The gray line in Figure 14.7 (c) corresponds to a single realization of ACF whereas the black line appears as a result of the ensemble averaging over a large number of random realizations of A_j in Eq. (14.6). It should be noted that both ACFs shown in Figure 14.7 (c) and Figure 14.7 (d) have a bell-shaped pedestal with a narrow peak on it. Central peaks of both ACFs are shown magnified in Figure 14.7 (e) and Figure 14.7 (f). It can readily be seen from Figure 14.7 (e) and Figure 14.7 (f) that there is a relatively minor but qualitative difference between "random" pulses Eq. (14.6) and noise-like pulses obtained within NLSE-based model Eqs. (14.1 and 14.2) which consists of the height of the ACF pedestal. In the proposed model of "random" pulses Eq. (14.6), the height of the ACF pedestal is equal to 0.5 (see Figure 14.7 (e)), indicating the completely random nature of radiation. However, for noise-like pulses obtained within an NLSE-based model (Eqs. 14.1, 14.2), the ACF pedestal is a bit higher (about 0.64 in height), suggesting the presence of some additional mode correlations inherent to noise-like pulses that are not taken into account by the proposed model Eq. (14.6).

Spectra of "random" pulses Eq. (14.6) and noise-like pulses obtained within NLSE-based model (Eqs. 14.1, 14.2) are shown in Figure 14.8 (a) and Figure 14.8 (c) respectively. In both cases, gray lines indicate single random realizations of the pulse spectrum, whereas black lines correspond to the result of ensemble averaging. Similar to the temporal intensity distribution, the optical spectrum of a single pulse is peaky. Experimentally measured spectra, as a rule, are smooth due to averaging over multiple successive pulses in a pulse train generated by a mode-locked laser in experiment. One can easily see completely different forms of ensemble-averaged spectra shown in Figure 14.8. Thus the spectrum of noise-like pulses obtained within the NLSE-based model (Eqs. 14.1, 14.2) and shown in Figure 14.8 (c) has a bell-shaped form whereas the spectrum of "random" pulses Eq. (14.3) shown in Figure 14.8 (a) is rectangular (Π-shaped). It should be stressed that this difference is not a drawback of the proposed model. Indeed, the model Eq. (14.6) can use any spectral shape $|A_j(\omega)|^2$ known from experiment or direct simulation of laser generation. We used a rectangular Π-shaped spectrum in Eq. (14.6) when we plotted Figure 14.8 (a) only for the sake of simplicity.

Finally, let us consider mode correlations that appear in NLSE-based simulations and in the model of "random" pulses, see Eq. (14.6). In what follows, we will use the coefficient of mode correlations γ calculated for a pair of modes in simulations, one of them is the central mode of the spectrum, another one has frequency detuning ν from the central spectral mode:

$$\gamma(\nu) = \gamma(A_\nu, A_0) = \frac{\left|\sum A_\nu A_0^*\right|}{\sqrt{\left(\sum |A_\nu|^2\right) \cdot \left(\sum |A_0|^2\right)}} \tag{14.7}$$

where A_ν and A_0 = complex amplitudes of spectral modes, one (A_ν) with frequency detuning ν from the center of the spectrum, the other (A_0) is the amplitude of the
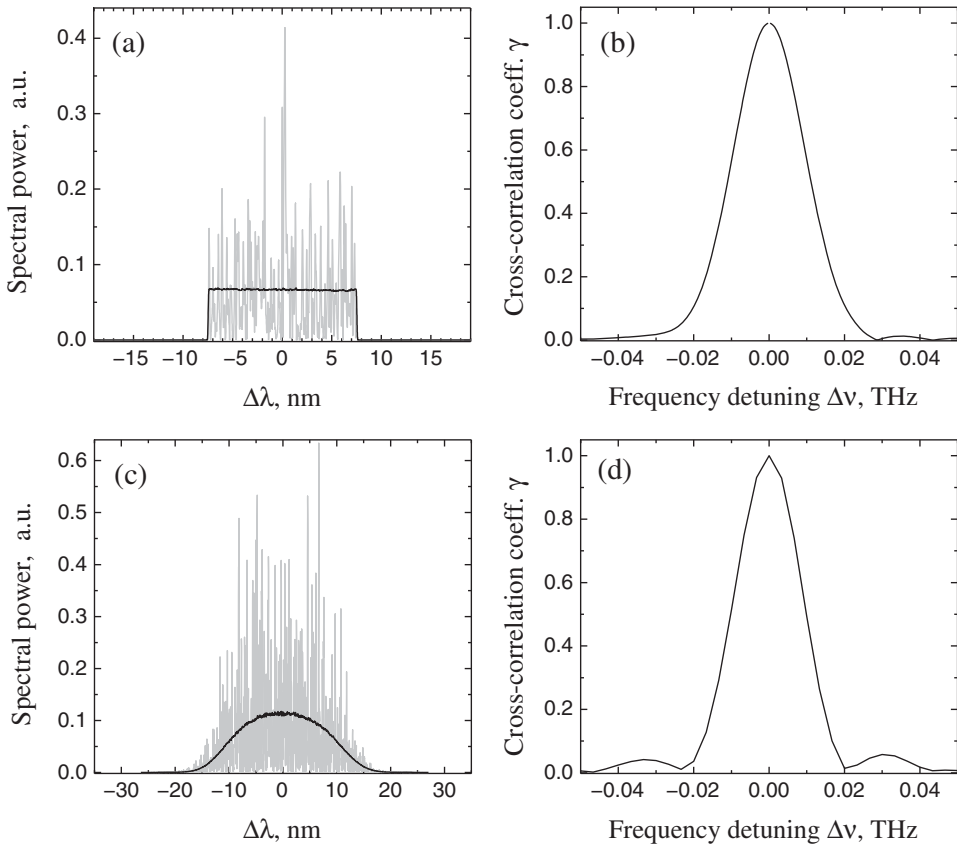
Figure 14.8 Spectra (a, c) and coefficient of mode correlations $\gamma(\Delta \nu, 0)$ (b, d) of "random" pulses (upper row a, b) and noise-like pulses (lower row c, d).

central mode in the generated spectrum. The graphs $\gamma(\nu)$ for "random" pulses Eq. (14.6) and noise-like pulses obtained within NLSE-based model (Eqs. 14.1, 14.2) are shown in Figures 14.8 (b) and 14.8 (d) respectively. The correlation coefficient of any variate with itself is equal to unity, $\gamma(\nu = 0) = 1$. Let us note that both graphs look similar. Adjacent spectral modes of both "random" and noise-like pulses are strongly correlated but the correlation coefficient drops rapidly down to 0 in a spectral area much narrower than the pulse bandwidth. The width of the spectral area of correlated modes is equal to the spectral width of pulse envelope both for "random" and noise-like pulses. It should be noted that different modes A_j in Eq. (14.6) were independent before being multiplied by $P(t)^{1/2}$, which was carefully checked in simulations. Thus, mode correlations of "random" pulses Eq. (14.6) appear as a result of pulse shaping.

14.4 Conclusion

Passively mode-locked fiber lasers based on artificial saturable absorption, such as nonlinear polarization evolution effect, NOLM/NALM, etc., possess a significant number of degrees of freedom (e.g., orientation angles of intra-cavity polarization elements and

the pump source power). Owing to these degrees of freedom, these lasers demonstrate a great variety of generation regimes differing from each other both qualitatively and in quantitative parameters (energy and duration of pulses, spectral width, etc.), which latter may vary by an order of magnitude and even more. For instance, along with "regular" pulses, passively mode-locked fiber lasers may also generate noise-like pulses (or double-scale lumps [37]), the terms used to designate wave-packets stochastically filled with short sub-pulses. The duration of these sub-pulses is usually within the femtosecond or sub-picosecond range, while their peak power may be a few times or even by an order of magnitude higher than the average peak power of the wave packet. Modeling of such lasers is more challenging and sensitive to the initial conditions [60]. The peculiar structure and unique properties of noise-like pulses make them very attractive in a number of applications, including nonlinear frequency conversion, imaging, and sensing systems. The parameters of such pulses, including duration, energy, and spectral width, may also vary within very broad limits. Moreover, due to highly nonlinear intra-cavity dynamics, the order of elements in the cavity may be important for the optimization of the laser system performance [61]. The proposed phenomenological model, assuming noise-like pulses to be the result of the superposition of uncorrelated modes with a given (freely chosen) spectral shape and temporal envelope, may be advantageous in modeling practical applications of noise-like pulses. Note that the double-scale clusters of pulses may be advantageous for the ablation applications similar to burst-mode operating lasers [62].

Acknowledgments

References

1 Hargrove, L.E., Fork, R.L., and Pollack, M.A. (1964) Locking of He–Ne laser modes induced by synchronous intracavity modulation. *Applied Physics Letters*, **5**, 4–5.

2 Ippen, E.P. Shank, C.V. and Dienes, A. (1972) Passive mode locking of the CW dye laser. *Applied Physics Letters* **21**, 348–350.

3 Alcock, I.P., Ferguson, A.I., Hanna, D.C., and Tropper, A.C. (1986) Mode-locking of a neodymium-doped monomode fibre laser. *Electronics Letters* **22** (5), 268–269.

4 Geister, G. and Ulrich, R. (1988) Neodymium-fibre laser with integrated-optic mode locker. *Optics Communications*, **68** (3), 187–189.

5 Kafka, J.D., Baer, T., and Hall, D.W. (1989) Mode-locked erbium-doped fiber laser with soliton pulse shaping. *Optics Letters*, **14** (22), 1269–1271.

6 Set, Y.S., Yaguchi, H., Tanaka, Y., and Jablonski, M. (2004) Laser mode locking using a saturable absorber incorporating carbon nanotubes. *Journal of Lightwave Technology*, **22**(1), 51–56.

7 Kieu, K. and Mansuripur, M. (2007) Femtosecond laser pulse generation with a fiber taper embedded in carbon nanotube/polymer composite. *Optics Letters*, **32** (15), 2242–2244.

8 Yamashita, S., Inoue, Y., Maruyama, S., *et al.* (2004) Saturable absorbers incorporating carbon nanotubes directly synthesized onto substrates and fibers and their application to mode-locked fiber lasers. *Optics Letters*, **29** (14), 1581–1583.

9 Wang, F., Rozhin, A.G., Scardaci, V., *et al.* (2008) Wideband-tuneable, nanotube mode-locked, fibre laser. *Nature Nanotechnology*, **3** (12), 738–742.

10 Schibli, T.R., Minoshima, K., Kataura, H., *et al.* (2005) Ultrashort pulse-generation by saturable absorber mirrors based on polymer-embedded carbon nanotubes. *Optics Express*, **13** (20), 8025–8031.

11 Kieu, K. and Wise, F.W. (2008) All-fiber normal-dispersion femtosecond laser. *Optics Express*, **16** (15), 11453–11458.

12 Song, Y.W., Yamashita, S., and Maruyama, S. (2008) Single-walled carbon nanotubes for high-energy optical pulse formation. *Applied Physics Letters*, **92** (2), 021115.

13 Bao, Q., Zhang, H., Wang, Y., *et al.* (2009) Atomic-layer graphene as a saturable absorber for ultrafast pulsed lasers. *Advanced Functional Materials*, **19** (19), 3077–3083.

14 Sun, Z., Hasan, T., Torrisi, F., *et al.* (2010) Graphene mode-locked ultrafast laser. *ACS Nano*, **4** (2), 803–810.

15 Zhang, H., Tang, D.Y., Zhao, L.M., Bao, Q.L., and Loh, K.P. (2009) Large energy mode locking of an erbium-doped fiber laser with atomic layer graphene. *Optics Express*, **17** (20), 17630–17635.

16 Zhang, H., Lu, S.B., Zheng, J., *et al.* (2014) Molybdenum disulfide (MoS2) as a broadband saturable absorber for ultra-fast photonics. *Optics Express*, **22** (6), 7249–7260.

17 Du, J., Wang, Q., Jiang, G., *et al.* (2014) Ytterbium-doped fiber laser passively mode locked by few-layer Molybdenum Disulfide (MoS2) saturable absorber functioned with evanescent field interaction. *Scientific Reports*, **4**, 6346.

18 Woodward, R.I. and Kelleher, E.J. (2015) 2D saturable absorbers for fibre lasers. *Applied Science*, **5** (4), 1440–1456.

19 Mao, D., Zhang, S., Wang, Y., *et al.* (2015) WS_2 saturable absorber for dissipative soliton mode locking at 1.06 and 1.55 μm. *Optics Express*, **23** (21), 27509–27519.

20 Zhao, C., Zhang, H., Qi, X., *et al.* (2012) Ultra-short pulse generation by a topological insulator based saturable absorber. *Applied Physics Letters*, **101** (21), 211106.

21 Yu, H., Zhang, H., Wang, Y., *et al.* (2013) Topological insulator as an optical modulator for pulsed solid-state lasers. *Laser Photonics Review*, **7** (6), L77–L83.

22 Keller, U., Miller, D.A.B., Boyd, G.D., *et al.* (1992) Solid-state low-loss intracavity saturable absorber for Nd:YLF lasers: an antiresonant semiconductor Fabry-Perot saturable absorber. *Optics Letters*, **17** (7), 505–507.

23 Keller, U., Weingarten, K.J., Kärtner, F.X., *et al.* (1996) Semiconductor saturable absorber mirrors (SESAM's) for femtosecond to nanosecond pulse generation in solid-state lasers. *IEEE Journal of Selected Topics in Quantum Electronics*, **2** (3), 435–453.

24 Okhotnikov, O.G., Jouhti, T., Konttinen, J., Karirinne, S., and Pessa. M. (2003) 1.5-μm monolithic GaInNAs semiconductor saturable-absorber mode locking of an erbium fiber laser. *Optics Letters*, **28** (5), 364–366.

25 Okhotnikov, O.G., Gomes, L., Xiang, N., Jouhti, T., and Grudinin, A.B. (2003) Mode-locked ytterbium fiber laser tunable in the 980–1070-nm spectral range. *Optics Letters*, **28** (17), 1522–1524.

26 Okhotnikov, O., Grudinin, A., and Pessa, M. (2004) Ultra-fast fibre laser systems based on SESAM technology: new horizons and applications. *New Journal of Physics*, **6** (1), 177–198.

27 Doran, N.J. and Wood, D. (1988) Nonlinear-optical loop mirror. *Optics Letters*, **13** (1), 56–58.

28 Fermann, M.E., Haberl, F., Hofer, M., and Hochreiter, H. (1990) Nonlinear amplifying loop mirror. *Optics Letters*, **15** (13), 752–754.

29 Matsas, V.J., Newson, T.P., Richardson, D.J., and Payne, D.N. (1992) Self-starting, passively mode-locked fibre ring soliton laser exploiting non-linear polarisation rotation. *Electronics Letters*, **28** (15), 1391–1393.

30 Kobtsev, S., Kukarin, S., and Fedotov, Y. (2008) Ultra-low repetition rate mode-locked fiber laser with high-energy pulses. *Optics Express*, **16** (26), 21936–21941.

31 Nyushkov, B.N., Denisov, V.I., Kobtsev, S.M., *et al*. (2010) Generation of 1.7-μJ pulses at 1.55 μm by a self-modelocked all-fiber laser with a kilometers-long linear-ring cavity. *Laser Physics Letters*, **7** (9), 661–665.

32 Kobtsev, S.M., Kukarin, S.V., Smirnov, S.V., and Fedotov, Y.S. (2010) High-energy mode-locked all-fiber laser with ultralong resonator. *Laser Physics*, **20** (2), 351–356.

33 Ivanenko, A., Turitsyn, S., Kobsev, S., and Dubov, M. (2010) Mode-locking in 25-km fiber laser. *European Conference on Optical Communication (ECOC)*, 1–3.

34 Fedotov, Y.S., Ivanenko, A.V., Kobtsev, S.M., and Smirnov, S.V. (2014) High average power mode-locked figure-eight Yb fibre master oscillator. *Optics Express*, **22** (25), 31379–31386.

35 Smirnov, S.V., Kobtsev, S.M., Kukarin, S.V. and Turitsyn, S.K. (2011) *Mode-Locked Fibre Lasers with High-Energy Pulses*. InTech, Moscow. Chapter 3.

36 Smirnov, S., Kobtsev, S., Kukarin, S., and Ivanenko, A. (2012) Three key regimes of single pulse generation per round trip of all-normal-dispersion fiber lasers mode-locked with nonlinear polarization rotation. *Optics Express*, **20** (24), 27447–27453.

37 Kobtsev, S., Kukarin, S., Smirnov, S., Turitsyn, S., and Latkin, A. (2009) Generation of double-scale femto/pico-second optical lumps in mode-locked fiber lasers. *Optics Express*, **17** (23), 20707–20713.

38 Smirnov, S., Kobtsev, S., and Kukarin, S. (2014) Efficiency of non-linear frequency conversion of double-scale pico-femtosecond pulses of passively mode-locked fiber laser. *Optics Express*, **22** (1), 1058–1064.

39 G. P. Agrawal (2001) *Nonlinear Fiber Optics*, 3rd ed., Academic Press, San Diego, CA.

40 Komarov, A., Leblond, H., and Sanchez, F. (2005) Multistability and hysteresis phenomena in passively mode-locked fiber lasers. *Physical Review A*, **71**, 053809.

41 Horowitz, M., Barad, Y., and Silberberg, Y. (1997) Noise-like pulses with a broadband spectrum generated from an erbium-doped fiber laser. *Optics Letters*, **22** (11), 799–801.

42 Pottiez, O., Grajales-Coutiño, R., Ibarra-Escamilla, B., Kuzin, E.A., and Hernández-García, J.C. (2011) Adjustable noise-like pulses from a figure-eight fiber laser. *Applied Optics*, **50** (25), E24–E31.

43 Nie, B., Parker, G., Lozovoy, V.V., and Dantus, M. (2014) Energy scaling of Yb fiber oscillator producing clusters of femtosecond pulses. *Optical Engineering*, **53** (5), 051505.

44 Kobtsev, S., Kukarin, S., Smirnov, S., and Ankudinov, I. (2014) Cascaded SRS of single- and double-scale fiber laser pulses in long extra-cavity fiber. *Optics Express*. **22** (17), 20770–20775.

45 Kobtsev, S., Kukarin, S., and Smirnov, S. (2015) Supercontinuum from single- and double-scale fiber laser pulses in long extra-cavity P2O5-doped silica fiber. *Proceedings of the SPIE*, **9347**, 93471X-1.

46 Kobtsev, S., Kukarin, S., and Smirnov, S. (2010) All-fiber high-energy supercontinuum pulse generator. *Laser Physics*, **20** (2), 375–378.

47 Hernandez-Garcia, J.C., Pottiez, O., and Estudillo-Ayala, J.M. (2012) Supercontinuum generation in a standard fiber pumped by noise-like pulses from a figure-eight fiber laser. *Laser Physics*, **22** (1), 221–226.

48 Zaytsev, A., Lin, C., You, Y., *et al.* (2013) Supercontinuum generation by noise-like pulses transmitted through normally dispersive standard single-mode fibers. *Optics Express*, **21** (13), 16056–16062.

49 Lin, S., Hwang, S., and Liu, J. (2014) Supercontinuum generation in highly nonlinear fibers using amplified noise-like optical pulses. *Optics Express*, **22** (4), 4152–4160.

50 Kobtsev, S., Kukarin, S., Smirnov, S., and Fedotov, Y. (2010) Ultra-wide-tunable fibre source of femto- and picosecond pulses based on intracavity Raman conversion. *Proceedings of the SPIE*, **7580**, 758023.

51 Smirnov, S.V., Ania-Castanon, J.D., Ellingham, T.J., *et al.* (2006) Optical spectral broadening and supercontinuum generation in telecom applications. *Optical Fiber Technology*, **10** (2), 122–147.

52 Smirnov, S.V., Kobtsev, S.M., and Kukarin, S.V. (2015) Linear compression of chirped pulses in optical fibre with large step-index mode area. *Optics Express*, **23** (4), 3914–3919.

53 Kobtsev, S.M. and Smirnov, S.V. (2005) Modelling of high-power supercontinuum generation in highly nonlinear, dispersion shifted fibers at CW pump. *Optics Express*, **13** (18), 6912–6918.

54 Kobtsev, S.M. and Smirnov, S.V. (2008) Temporal structure of a supercontinuum generated under pulsed and CW pumping. *Laser Physics*, **18** (11), 1260–1263.

55 Kobtsev, S.M. and Smirnov, S.V. (2008) Influence of noise amplification on generation of regular short pulse trains in optical fibre pumped by intensity-modulated CW radiation. *Optics Express*, **16** (10), 7428–7434.

56 Kobtsev, S.M., and Smirnov, S.V. (2006) Coherent properties of super-continuum containing clearly defined solitons. *Optics Express*, **14** (9), 3968–3980.

57 Kobtsev, S.M., Kukarin, S.V., Fateev, N.V. and Smirnov, S.V. (2005) Coherent, polarization and temporal properties of self-frequency shifted solitons generated in polarization-maintaining microstructured fibre. *Applied Physics B*, **81** (2), 265–269.

58 Kobtsev, S.M., Kukarin, S.V., Fateev, N.V., and Smirnov, S.V. (2004) Generation of self-frequency-shifted solitons in tapered fibers in the presence of femtosecond pumping. *Laser Physics*, **14** (5), 748–751.

59 Churkin, D.V., Sugavanam, S., Tarasov, N., *et al.* (2015) Stochasticity, periodicity and localized light structures in partially mode-locked fibre lasers. *Nature Communications*, **6**, 7004.

60 Yarutkina, I.A., Shtyrina, O.V., Fedoruk, M.P., and Turitsyn, S.K. (2013) Numerical modeling of fiber lasers with long and ultra-long ring cavity. *Optics Express*, **21**, 12942–12950.

61 Shtyrina, O.V., Yarutkina, I.A., Skidin, A., Fedoruk, M.P., and Turitsyn, S.K. (2015) Impact of the order of cavity elements in all-normal dispersion ring fiber lasers. *IEEE Photonics Journal*, **7**(2) 1501207.

62 Kalaycıoğlu, H., Akçaalan, Ö., Yavaş, S., Eldeniz, Y.B., and Ilday, F.Ö. (2015) Burst-mode Yb-doped fiber amplifier system optimized for low-repetition-rate operation. *Journal of the Optical Society of America B*, **32**, 900–906.